Materials Transactions, Vol. 65, No. 5 (2024) pp. 481 to 486

Temperature Dependence of Nanoindentation-Induced Deformation Dynamics in Zr-Based Bulk Metallic Glass

Silvia Pomes[1,2], Nozomu Adachi[3], Masato Wakeda[1] and Takahito Ohmura[1,2,*]

[1]*Research Center for Structural Materials, National Institute for Materials Science, Tsukuba 305-0047, Japan*
[2]*Department of Materials Science and Engineering, Graduate School of Engineering, Kyushu University, Fukuoka 819-0395, Japan*
[3]*Department of Mechanical Engineering, Toyohashi University of Technology, Toyohashi 441-8580, Japan*

Nanoindentation-induced deformation in Zr-based bulk metallic glasses in distinct structural states was studied over a broad temperature range, both below and above the glass transition temperature. These findings emphasize the occurrence of a predominant deformation mechanism, identified as a percolation or diffusion process, triggered by exceeding a chemical and topological short-range order-insensitive energy barrier. [doi:10.2320/matertrans.MT-MBW2023002]

(Received November 22, 2023; Accepted January 31, 2024; Published February 16, 2024)

Keywords: *bulk metallic glass, nanoindentation, deformation, mechanical properties, glass transition temperature, percolation/diffusion*

1. Introduction

Bulk metallic glasses (BMGs) have garnered attention as promising materials for structural applications primarily because of their exceptional mechanical properties, including high elastic limit, remarkable strength, and hardness.[1,2] In addition, BMGs have a distinctive microstructure that lacks long-range order and exhibits regions with diverse geometrical constraints and degrees of frustration. These structural characteristics contribute to their peculiar deformation response, which is significantly influenced by environmental factors, particularly the temperature. The structure of BMGs constantly evolves through atomic rearrangements and free-volume redistribution[3,4] during deformation, driven by the supplied mechanical and thermal energy. Notably, the mechanical performance and inherent microstructure of BMGs are significantly influenced by their glass transition temperature (T_g). Indeed, T_g exhibits a linear relationship with the activation energy for β-relaxation.[5] Moreover, at a specific temperature, denoted as T_x, above T_g, BMGs undergo a crystallization process, leading to further alterations in the mechanical properties of the alloy. Furthermore, deformation in BMGs can manifest as either homogeneous or inhomogeneous flow, contingent on both temperature range and strain rate. Homogeneous flow is expected in the range $0.6-1\ T_g$.[6–8] Nevertheless, the temperature range for each type of flow is significantly impacted by the strain rate: a slower strain rate corresponds to a lower transition temperature from inhomogeneous to homogeneous flow.[9]

Given the heterogeneous and unstable microstructure of BMGs, nanoindentation testing is a robust approach for assessing the mechanical properties at a highly localized scale, offering both time and cost efficiency.[10] Furthermore, owing to the advancements in thermal management techniques, nanoindentation can be conducted at elevated temperatures,[11] providing valuable insights into the underlying deformation processes of BMGs. Recently, Ghodki *et al.*[12] employed high-temperature nanoindentation to study the bulk deformation behavior of a Zr-based BMG and discussed it based on the shear transformation zone concept. In their study, testing was conducted below the T_g and featured indentation marks in the range of tens of micrometers. However, it has been demonstrated that studying the effects of more localized deformation, resulting in indentation marks on the scale of hundreds of nanometers, can aid in identifying elemental deformation dynamics.[13] Additionally, expanding the temperature range of investigation to include temperatures above T_g would serve the same purpose.

The high-temperature deformation of Zr-based BMG was studied through compression testing by Bletry *et al.*[14] The deformation behavior was interpreted in terms of the free-volume model, which attributed plasticity to the cooperative motion of a group of a few tens of atoms. Although it is widely accepted that deformation in BMGs involves the reorganization of a chemical short-range order (CSRO) and topological short-range order (TSRO), the underlying dynamics and process variability concerning the testing environment temperature and structural state of the original samples remain unclear.

In this study, we performed nanoindentation tests at elevated-temperature on a Zr-based BMG in two distinct structural states. Our approach covers a wide range of testing temperatures, from room temperature to the crystallization temperature, including T_g. We conducted numerous tests to ensure the statistical significance of the overall temperature dependence of the mechanical properties and provide insights into potential deformation mechanisms.

2. Experimental Procedure

Two samples of $Zr_{50}Cu_{40}Al_{10}$ at% BMG were used in the as-cast and as-relaxed structural states. The BMG was produced in the form of rods with a diameter of 10 mm by arc melting and tilt casting, as elaborately described in previous studies.[15,16] The as-cast sample was annealed for 3 h at 40 K below the $T_g = 693$ K (420°C) to obtain the as-relaxed sample. Disks with a thickness of 2 mm were

*Corresponding author, E-mail: OHMURA.Takahito@nims.go.jp

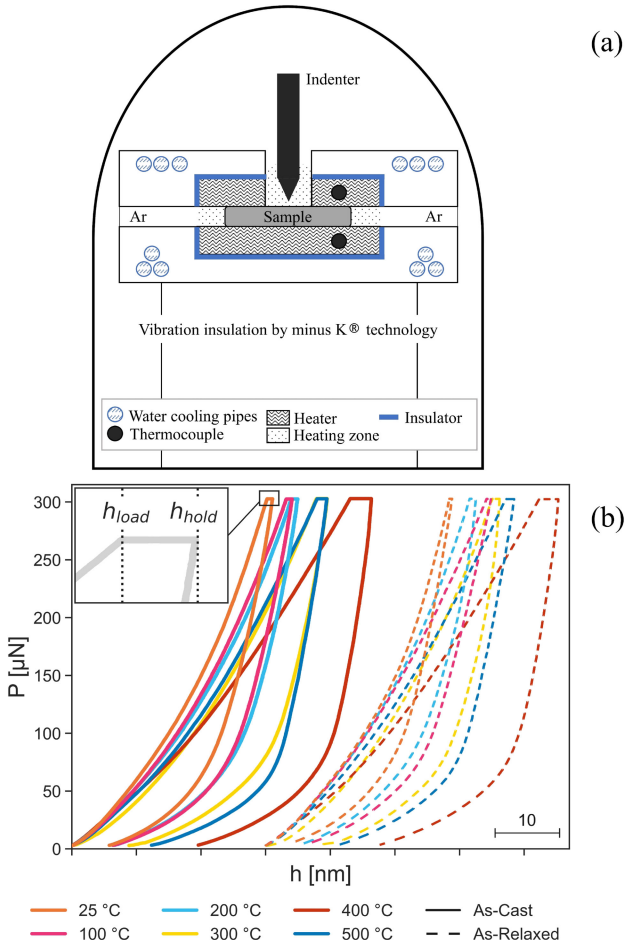

Fig. 1 (a) Schematic of high-temperature nanoindentation testing in an inert-atmosphere machine.[15] (b) Load versus displacement plot of averaged nanoindentation curves for as-cast (continuous line) and as-relaxed samples (dashed line). Tests are performed at 25°C, 100°C, 200°C, 300°C, 400°C, and 500°C. As-relaxed sample curves are horizontally shifted. The inset shows the definition of h_{load} and h_{hold} parameters as the indentation depth recorded at the end of loading and holding segments, respectively.

obtained from the rod. The disk samples were mechanically polished using sandpaper and diamond suspension with a particle size of up to 1 μm. Finally, a sol–gel Al_2O_3 suspension with a particle size of 0.05 μm was used to remove the damaged surface layer resulting from mechanical polishing. The surface roughness (RMS) was 1 nm after final polishing. The nanoindentation was conducted using a prototype high-temperature experimental setting in inert atmosphere. Details of the device are described elsewhere.[17] A schematic diagram of the machine is shown in Fig. 1(a). A high-temperature-stage nanoindentation testing setup (Bruker Co.) was used, which was placed in a vacuum chamber on a vibration isolation stage (Minus K Technology Inc.). The vacuum chamber was equipped with gas inlets that allowed for the control and introduction of gases, along with an external cooling system. Prior to heating, the vacuum chamber undergoes cyclic evacuation to a pressure of 1.33 mPa (10^{-5} Torr) and is subsequently backfilled with a mixture of 98% argon gas and 2% H_2 to minimize the oxygen levels. In the experimental setup, the sample was positioned between two independently controlled heaters with heating applied simultaneously from the top and bottom. The dual heating configuration ensures uniform temperature distribution within the sample, with a slow heating rate (≥10°C/min). The indenter tip was positioned 100 μm above the sample surface and passively heated. Both the tip and sample were maintained at the testing temperature for 1 h before the measurements began, to improve the thermal stability. Tests were performed in the load control mode with a peak load of 300 μN and a symmetrical loading and unloading rate of 10 μN/s and holding time of 10 s at the peak load. The distance between the test locations was 5 μm to ensure no interaction between the induced strain fields. For statistical significance, 125 tests were performed at each temperature, resulting in 750 tests in total on one sample.[18] Nanoindentation tests were performed with a sharp Berkovich tip, with tip radius $R_i \sim 290$ nm, at 25°C, 100°C, 200°C, 300°C, 400°C, and 500°C. The collected data were analyzed using Python.[19,20]

3. Results and Discussions

Figure 1(b) illustrates load P versus displacement h plots, with each curve representing an average of 125 tests. The averaging of the curves is performed as the measured hardness values displayed no discernible trend with respect to testing time. This observation suggests that the technical time required to conduct the tests did not exert a substantial influence on the mechanical properties. The curves of as-relaxed sample were shifted horizontally to enhance the clarity of visualization. The inset in the upper-left corner shows the definitions of h_{load} and h_{hold} parameters corresponding to the indentation depths recorded at the end of the loading and holding segments, respectively. In both samples, h_{load} and h_{hold} increased with temperature, peaking at 400°C (red curves) and showing a decreased value at 500°C (blue curves). Figure 2(a) shows the hardness values of the as-cast and as-relaxed samples at different testing temperatures. Compared to previous studies, the hardness values obtained were higher, which might be due to the sharp tip or strain-rate sensitivity at low peak loads.[21] Moreover, as previously reported,[22] structures such as oxides may have formed in conjunction with zirconium, potentially impacting the calculated hardness at the tested locations. Due to this influence, the detailed discussion of the computed hardness values is omitted, in favor of a more in-depth discussion on their trend.

The light-blue hatched area indicates the temperature range of 200°C to 400°C where softening is observed. It is noted that this area is included in the 0.8 T_g (~ 336°C) to T_g temperature range, previously reported as range for homogeneous flow in bulk metallic glasses.[6] Furthermore, the range where softening is observed also falls in the 0.6 T_g (~ 142°C) to T_g temperature span, reported by Argon as domain for homogeneous flow in metallic glasses.[7] However, it may be possible that, even at the same temperature, deformation may exhibit flows with varying degrees of uniformity, due to the complexity introduced by the amorphous samples. In fact, highly localized deformation processes might not be exclusively dictated by temperature and loading rate but could also be contingent on specific

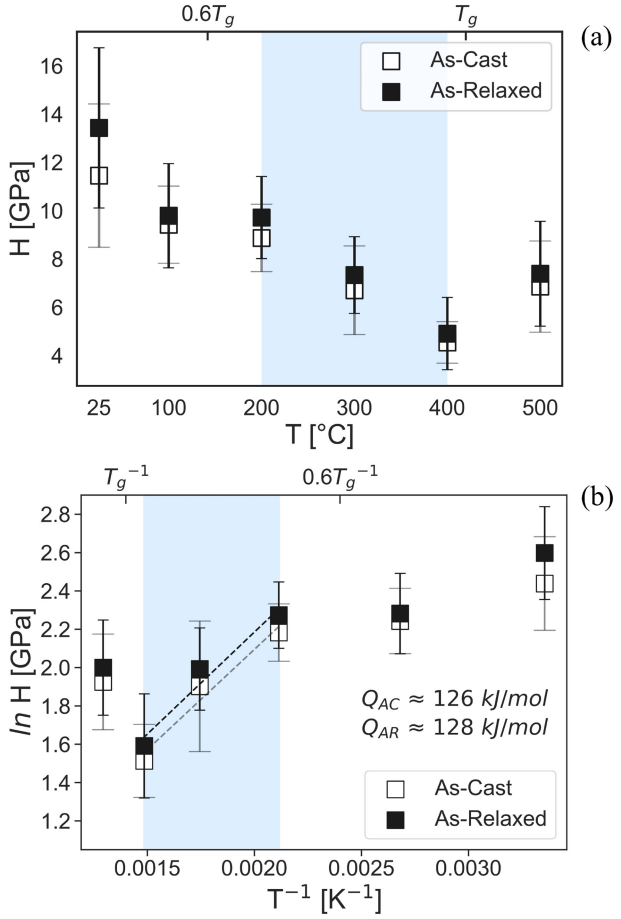

Fig. 2 (a) Estimated hardness for as-cast and as-relaxed samples at different testing temperatures and (b) estimation of activation energy for softening in the homogeneous flow range.

testing location. In this work, the temperature range reported by Schuh *et al.*[6] and Argon[7] is regarded as potential range for homogeneous flow based on the absence of any detectable serrated flow in our tests. Furthermore, the local variations can be averaged due to the collection of a large dataset.

The overall trend of hardness confirms the observations made for the averaged curves in Fig. 1(b), i.e., the mean values of hardness exhibited a decreasing trend, reaching a minimum at 400°C, near T_g, followed by higher values at 500°C. At 25°C, the wider standard deviation can be attributed to the microstructural heterogeneity, resulting in regions with different degrees of atomic mobility. Conversely, at 500°C, the increased hardness value, compared to 400°C, could be attributed to microstructural changes occurring within the supercooled region, encompassing the temperature range between T_g and T_x. The supercooled region is characteristic of each alloy and typically spans the temperature range of 40 K–90 K.[23] Considering the T_g of the present alloy as 420°C, it can be reasonably assumed that the T_x may fall within the range of 460°C to 510°C. This estimate is consistent with previous experimental evaluations of alloys with the same composition, with $T_g = 706$ K (433°C) and $T_x = 792$ K (519°C).[24–26] Hence, crystallization processes might affect the hardness values measured at 500°C.

Overall, the as-relaxed sample exhibited a higher hardness than its as-cast counterpart, which can be attributed to the increased energetic stability of the microstructure and the lower volume fraction of free-volume within the sample.

The softening observed at temperatures below the T_g can be attributed to a deformation process activated upon reaching a certain activation energy threshold. Figure 2(b) shows the estimation of the activation energy for softening using the method adopted by Wesseling *et al.*:[8]

$$H^n \propto exp(Q/RT). \quad (1)$$

The activation energy coincides with the slope of the dashed lines in Fig. 2(b) under a condition of $n = 1$.

As proposed in the previous work,[8] n is considered equal to 1 because the temperature range in this work is consistent with the range for homogeneous flow[6,7] and homogenous flow usually corresponds to a Newtonian flow in metallic glasses.[7] Typically, as commonly done in uniaxial compression testing, Newtonian flow is assessed by evaluating the induced strain rate dependency. However, in nanoindentation, the indenter induces a complex stress state, encompassing both compression and shear components with corresponding compression and shear strain rates. Furthermore, in the context of nanoindentation testing, a direct observation of Newtonian viscous flow in the volume beneath the indenter presents technological challenges. For these reasons, the method proposed by Wesseling *et al.*[8] is considered. They performed microhardness Vickers tests at elevated temperature and directly evaluated the activation energy for softening from the indentation data under the assumption of a Newtonian flow. This approach can be applied to our nanoindentation study offering a valuable perspective on the material behavior under the complex stress conditions induced by the indenter.

The estimated activation energies of the as-cast and as-relaxed samples were 126 and 128 kJ/mol, respectively. These results suggest that the initial structural state does not influence deformation dynamics at elevated temperatures. The obtained values were compared with an estimate of the activation energy for β-relaxation, obtained as $E_\beta = 26(\pm 2)RT_g$, where R is the gas constant.[5] Hence, in the case of the studied alloy, E_β falls within the range of 138–161 kJ/mol. Although slightly lower, the estimated activation energies for softening were comparable to the potential range of activation energies for β-relaxation. Generally, β-relaxation is regarded as a local atomic rearrangement achieved through short-range diffusion.[27] However, Gao *et al.*[28] recently questioned the local nature of β-relaxation dynamics and explored this phenomenon in various BMGs. They emphasized that β-relaxation corresponds to the percolation of mobile atomic clusters and revealed a universal activation volume, expressed as a percentage of activated atoms. Considering both interpretations, it is reasonable to expect that the structural states of a sample do not influence the energy barrier of such dynamics. For the same alloy composition, the distinction between the as-cast and as-relaxed states lies in their CSRO and TSRO, implying that the enthalpy barrier for mobilizing atoms in unstable regions would likely be the same. Eventually, the weakest atomic arrangements, identified as non-pentagon configurations in the TSRO,[29] would be activated and constitute the mobile clusters.

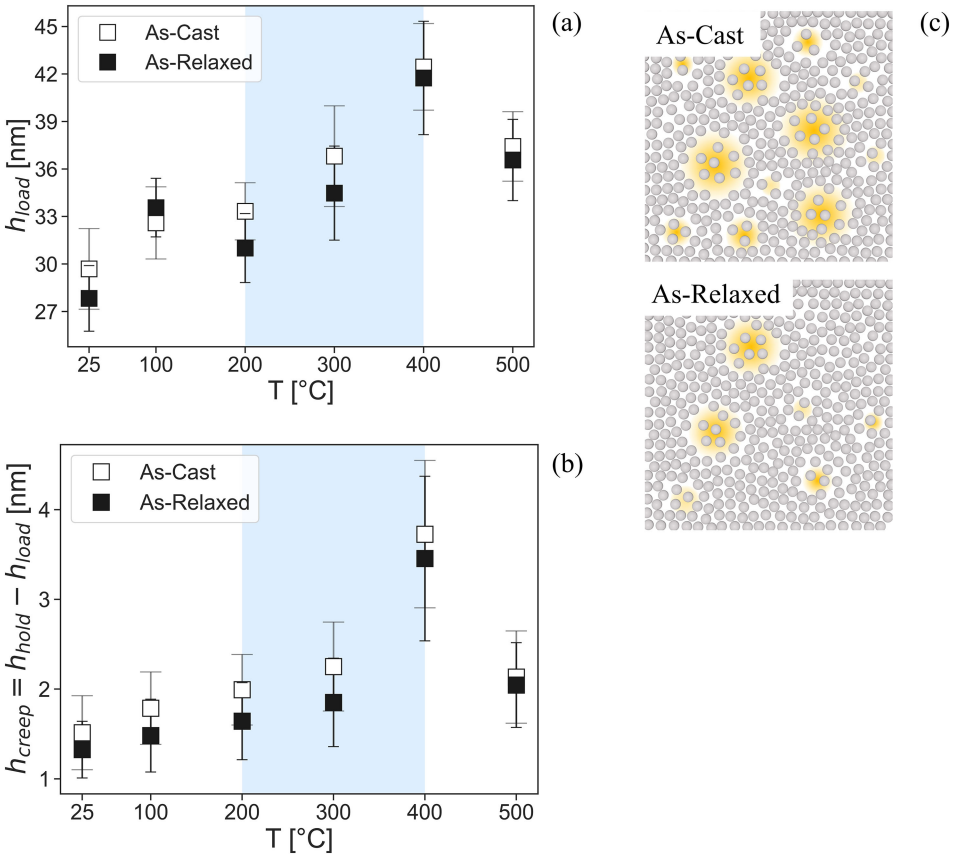

Fig. 3 Analysis of indentation depths, (a) h_{load} and (b) h_{creep} (P = constant), reveal deformation is favored in the as-cast sample. (c) Qualitative schematics of the atomistic structure of as-cast (top) and as-relaxed (bottom) samples. Unstable regions are represented in yellow and they are more abundant in the as-cast sample.

To further examine the effects of temperature on the deformation processes specific to the loading and holding stages, the trends of h_{load} and length of the holding segment, $h_{creep} = h_{hold} - h_{load}$, are analyzed in Fig. 3(a) and 3(b), respectively. In Fig. 3(a), the maximum indentation depth at loading increases in both samples with respect to temperature and exhibits a peak at 400°C. Similarly, in Fig. 3(b), h_{creep} increases with the temperature until its peak at 400°C. At 500°C, both samples exhibited a lower, comparable value. Notably, the observable trends exhibited similarities between the samples and the two plots, as shown in Fig. 3. The observed consistent patterns suggested a common dominant deformation dynamic, possibly identifiable as either a percolation or a diffusion process. Indeed, the overshadowing of load effects by diffusion processes has also been reported through creep strain rate sensitivity analysis of a Zr-based BMG tested below its T_g.[12)]

However, Fig. 3(a) displays a less smooth distribution compared to Fig. 3(b), which can be attributed to the presence of multiple mechanisms in the loading process, including displacive ones, acting synergistically during the loading stage of nanoindentation. As the applied load increases, the volume influenced by the applied stress also increases, leading to the involvement of more defects and free-volume regions in the energy dissipation process. Figure 3(c) provides a qualitative schematic of the atomistic structure of as-cast (top) and as-relaxed (bottom) samples with unstable regions represented in yellow. However, during the holding time, the deformation volume is predominantly established, and the eventual activation and percolation of atomic clusters are facilitated by high-temperature-induced structural vibrations under a constant applied load.

This rationale is applicable to both samples. However, as shown in Fig. 3(a) and 3(b), it translates into larger displacements in the as-cast sample, due to its higher volume fraction of unstable regions, as depicted in Fig. 3(c).

The smaller displacements recorded at 500°C in both samples may be attributed to the proximity of the testing temperature to the T_x range; the indenter motion may be hindered by newly formed structures.

To gain an additional understanding of the underlying mechanisms governing deformation in the holding stage, the evolution of displacement was analyzed with respect to time, as shown in Fig. 4(a). The averaged experimental data replotted from Fig. 1(b) are indicated by circular and diamond markers for the as-cast and as-relaxed samples, respectively. The fitting curves were obtained from the following empirical equation:[30,31)]

$$h(t) = h_0 + at + b(t - t_0)^c \tag{2}$$

considering a, b, and c as the fitting parameters, and h_0 and t_0 as the origin of the plot, marked with solid and dashed lines for the as-cast and as-relaxed samples, respectively. The coefficient of determination value was higher than 0.97 for all curves except for the tests performed on the as-relaxed sample at 25°C (0.929) and 100°C (0.964). Figure 4(b)

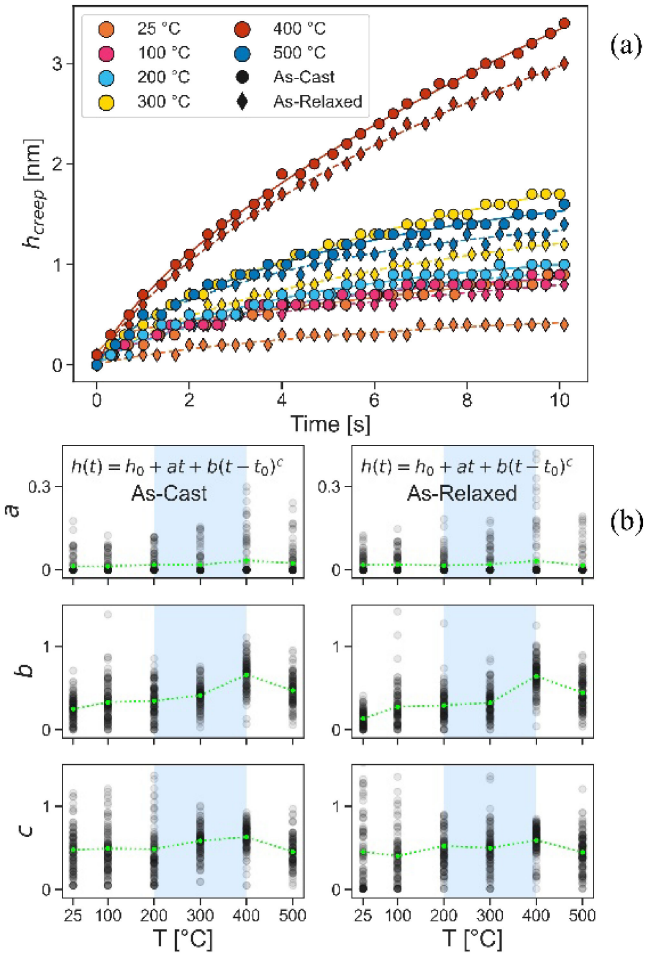

Fig. 4 (a) Creep time versus displacement plot of representative nanoindentation averaged holding segments. The as-cast and as-relaxed samples are represented by circular markers with a continuous fitting line and diamond markers with a dashed fitting line, respectively. (b) Fitting parameters vs. temperature. The parameters evaluated for each test are indicated in black, while the mean values are displayed in green.

illustrates the estimated fitting parameters for each test (depicted in black) along with the average values (presented in green). Overall, a steady-state stage with parameter a for creep was not clearly detectable. This suggests the occurrence of an unstable deformation behavior in the early stage of deformation under constant applied load. While the overall deformation and energy dissipation may demonstrate a clear temperature dependence, as shown in Fig. 3(b), the specific local dynamics underlying these processes might still exhibit less predictable and less stable behavior at each testing location.

The fitting parameters exhibited significant variability, primarily attributed to structural fluctuations within the samples. Specifically, the parameter a governing the linear term in eq. (2) exhibited values close to zero, as shown in Fig. 4(b). However, the power-law term in eq. (2) becomes linear when the exponent, which is the fitting parameter c, is approximately unity. This applies to tests conducted at 400°C, where the estimated fitting parameters show higher and less sparse values, overall. This phenomenon may be attributed to the proximity of the testing temperature to T_g, leading to increased atomic mobility and potential enhancement of the diffusive processes.

4. Conclusion

In summary, we investigated the deformation behavior of $Zr_{50}Cu_{40}Al_{10}$ bulk metallic glass ($T_g = 420$°C) in a comprehensive temperature range, encompassing 25°C, 100°C, 200°C, 300°C, 400°C, and 500°C, via nanoindentation testing in an inert atmosphere. The following key conclusions were drawn:

(1) The estimated hardness decreases with increasing testing temperature and reaches a minimum in proximity of T_g at 400°C.
(2) The estimated activation energies for softening were nearly identical for both samples, suggesting that the underlying physical dynamics were not affected by the initial structural state of the bulk samples.
(3) At 500°C, the hardness value increases compared with that at 400°C. This may be attributed to the higher resistance to atomic motion caused by crystallization.
(4) h_{load} and h_{creep} revealed similar temperature-dependent trends, which suggest that the same diffusive deformation mechanism may be predominant during both testing stages.
(5) Larger h_{creep} values were recorded in the as-cast sample due to the higher volume fraction of unstable regions.

Acknowledgments

S.P. is thankful for experimental support by Nakagawa Eri.

REFERENCES

1) W. Klement, R.H. Willens and P. Duwez: Nature **187** (1960) 869–870.
2) M.F. Ashby and A.L. Greer: Scr. Mater. **54** (2006) 321–326.
3) A.L. Greer and F. Spaepen: Ann. N. Y. Acad. Sci. **371** (1981) 218–237.
4) F. Spaepen: Scr. Mater. **54** (2006) 363–367.
5) L. Hu and Y. Yue: J. Phys. Chem. C **113** (2009) 15001–15006.
6) C.A. Schuh, A.C. Lund and T.G. Nieh: Acta Mater. **52** (2004) 5879–5891.
7) A.S. Argon: Acta Metall. **27** (1979) 47–58.
8) P. Wesseling, T.G. Nieh, W.H. Wang and J.J. Lewandowski: Scr. Mater. **51** (2004) 151–154.
9) B. Yang, J. Wadsworth and T.-G. Nieh: Appl. Phys. Lett. **90** (2007) 061911.
10) T. Ohmura: *Plast. Concept*, Nanomechanical Characterization of Metallic Materials, (Springer Nature, 2022) pp. 157–195.
11) J.M. Wheeler, D.E.J. Armstrong, W. Heinz and R. Schwaiger: Curr. Opin. Solid State Mater. Sci. **19** (2015) 354–366.
12) N. Ghodki, M. Sadeghilaridjani and S. Mukherjee: J. Non-Cryst. Solids **576** (2022) 121221.
13) S. Pomes, N. Adachi, M. Wakeda and T. Ohmura: Scr. Mater. **237** (2023) 115713.
14) M. Bletry, P. Guyot, J.J. Blandin and J.L. Soubeyroux: Acta Mater. **54** (2006) 1257–1263.
15) Y. Yokoyama, H. Fredriksson, H. Yasuda, M. Nishijima and A. Inoue: Mater. Trans. **48** (2007) 1363–1372.
16) N. Adachi, Y. Todaka and T. Ohmura: MRS Commun. **11** (2021) 330–335.
17) J. Ruzic, I. Watanabe, K. Goto and T. Ohmura: Mater. Trans. **60** (2019) 1411–1415.
18) S. Nag, R.L. Narayan, J. Jang, C. Mukhopadhyay and U. Ramamurty: Scr. Mater. **187** (2020) 360–365.
19) C.R. Harris *et al.*: Nature **585** (2020) 357–362.
20) J.D. Hunter: Comput. Sci. Eng. **9** (2007) 90–95.
21) Q. Zhou, Y. Du, W. Han, Y. Ren, H. Zhai and H. Wang: Scr. Mater. **164** (2019) 121–125.
22) K.S. Nakayama, Y. Yokoyama, T. Sakurai and A. Inoue: Appl. Phys.

Lett. **90** (2007) 183105.
23) C. Suryanarayana and A. Inoue: *Bulk Metallic Glasses*, 2nd ed., (CRC Press, 2017).
24) Y. Yokoyama, Y. Akeno, T. Yamasaki, P.K. Liaw, R.A. Buchanan and A. Inoue: Mater. Trans. **46** (2005) 2755–2761.
25) F. Meng, K. Tsuchiya and Y. Yokoyama: Mater. Trans. **55** (2014) 220–222.
26) R. Yamada, N. Tanaka, W. Guo and J. Saida: Mater. Trans. **58** (2017) 1463–1468.
27) F. Zhu, H.K. Nguyen, S.X. Song, D.P.B. Aji, A. Hirata, H. Wang, K. Nakajima and M.W. Chen: Nat. Commun. **7** (2016) 11516.
28) L. Gao, Y. Sun and H.-B. Yu: Phys. Rev. B **108** (2023) 014201.
29) M. Wakeda, Y. Shibutani, S. Ogata and J. Park: Intermetallics **15** (2007) 139–144.
30) H. Li and A.H.W. Ngan: J. Mater. Res. **19** (2004) 513–522.
31) Y.J. Huang, J. Shen, Y.L. Chiu, J.J.J. Chen and J.F. Sun: Intermetallics **17** (2009) 190–194.